8-2020

Activation of TRPA1 nociceptor promotes systemic adult mammalian skin regeneration

Jenny J. WEI
University of Pennsylvania

Hali S. KIM
University of Pennsylvania

Casey A. SPENCER
University of Pennsylvania

Donna BRENNAN-CRISPI
University of Pennsylvania

Ying ZHENG
University of Pennsylvania

See next page for additional authors

HHS Public Access

Author manuscript

Sci Immunol. Author manuscript; available in PMC 2021 February 28.

Published in final edited form as:

Sci Immunol. 2020 August 28; 5(50): . doi:10.1126/sciimmunol.aba5683.

Activation of TRPA1 Nociceptor Promotes Systemic Adult Mammalian Skin Regeneration

Jenny J. Wei[1], **Hali S. Kim**[1], **Casey A. Spencer**[1], **Donna Brennan-Crispi**[1], **Ying Zheng**[1], **Nicolette M. Johnson**[1], **Misha Rosenbach**[1], **Christopher Miller**[1], **Denis H. Leung**[3], **George Cotsarelis**[1,4], **Thomas H. Leung**[1,2,4,*]

[1]Department of Dermatology, University of Pennsylvania School of Medicine, Philadelphia, PA US.

[2]Corporal Michael Crescenz Veterans Affairs Medical Center, Philadelphia, PA.

[3]Singapore Management University, Singapore.

[4]Institute for Regenerative Medicine, University of Pennsylvania.

Abstract

Adult mammalian wounds, with rare exception, heal with fibrotic scars that severely disrupt tissue architecture and function. Regenerative medicine seeks methods to avoid scar formation and restore the original tissue structures. We show that pharmacologic activation of the nociceptor TRPA1 on cutaneous sensory neurons reduces scar formation and can also promote tissue regeneration in three adult mouse models. Remarkably, local activation of TRPA1 induces tissue regeneration on distant untreated areas of injury, demonstrating a systemic effect. Activated TRPA1 stimulates local production of IL-23 by dermal dendritic cells, leading to activation of circulating dermal interleukin (IL)-17-producing γδ T cells. Genetic ablation of TRPA1, IL-23, dermal dendritic cells, or γδ T cells prevents TRPA1-mediated tissue regeneration. These results reveal a cutaneous neuroimmune-regeneration cascade triggered by topical TRPA1 activators that promotes adult mammalian tissue regeneration, presenting a new avenue for research and development of therapies for wounds and scars.

Introduction

Organisms repair injury through two biological processes: scar formation and tissue regeneration (1, 2). Scar formation results in fibrosis and loss of normal skin architecture and structures, such as hair follicles. In contrast, tissue regeneration results in full

*Correspondence to: thl@pennmedicine.upenn.edu.

Author contributions: T.H.L. generated the hypotheses, designed experiments, performed experiments, analyzed data, and wrote the manuscript. J.J.W., H.S.K., and C.A.S. designed experiments, performed experiments, analyzed data, and edited the manuscript. N.M.J. and D.B. performed experiments. D.H.L. performed the statistical analysis and edited the manuscript. C.M. and M.R. performed experiments and edited the manuscript. Y.Z. and G.C. performed WIHN experiments and edited the manuscript.

Competing interests: G.C. is a founder and member of the scientific advisory board of Follica. A provisional patent has been filed with the US Patent and Trademark Office regarding TRPA1 activation on reducing scar formation and promoting tissue regeneration.

Data and materials availability: All data is available in the main text or the supplementary materials. All materials will be shared, and request for materials should be addressed to thl@pennmedicine.upenn.edu.

reconstitution of all tissue-specific cellular subtypes and functional architecture without scar formation. Two well-established mouse models of tissue regeneration are ear hole closure and wound-induced hair neogenesis (WIHN) (3–7). Typically, through-and-through ear wounds in the mouse ear pinna heal with a scar and remain open. However, in certain mouse strains and genotypes, ear holes may close to less than 10% of the original wound size, with a small fraction achieving complete closure (8–12). The healed tissue exhibits re-establishment of original tissue architecture with no scar formation. WIHN is a model of adult mammalian tissue regeneration, where large full thickness wounds on mouse back skin may heal with *de novo* formation of hair follicles, sebaceous glands, and fat (7). The newly regenerated hair follicles are complex tissues with multiple cell types and a distinct stem cell compartment.

Results

Topical imiquimod reduces scar formation and promotes mammalian tissue regeneration

Inflammation plays mixed roles in tissue regeneration (13). To investigate whether inflammation promotes tissue regeneration, we screened using the ear hole injury model several compounds commonly known to induce skin inflammation. Interestingly, we observed a tissue regeneration phenotype after topical treatment with 5% imiquimod cream which was not seen after treatment with other agents (Fig. 1A, Fig. S1). To confirm that imiquimod was the active ingredient, we compounded imiquimod powder into Cetaphil® cream and reproduced the tissue regeneration phenotype (Fig. S1C). We used Cetaphil® cream as the control for subsequent experiments.

Imiquimod cream induces inflammation through stimulation of toll-like receptor 7 (TLR7). 5% imiquimod cream is commonly used in the clinic to topically treat skin cancer and warts, and small clinical case series have reported that topical imiquimod may reduce pathological scar formation in humans (14). In wild-type (WT) mice, we observed that topical application of 5% imiquimod cream 5 days per week, beginning one week prior to ear hole injury, promoted full closure of through-and-through 2mm punch wounds (Fig. 1A, 1B). Strikingly, this complete ear hole closure occurred more frequently than in previously reported ear hole regeneration-competent mouse strains (3, 4, 12). Hematoxylin and eosin (H&E) staining of wound edge tissue from control-treated WT mice revealed horizontally oriented fibroblasts and glassy thickened collagen, indicating tissue fibrosis and scar formation (Fig. 1C, 1D). Opposing cartilage end plates remained approximately 2mm apart, confirming the absence of cartilage regeneration. By contrast, H&E staining on healed tissue from imiquimod-treated WT mice revealed normal tissue architecture, with hair follicles, sebaceous glands, and subcutaneous fat (Fig. 1D, black arrows denote new hair follicles and sebaceous glands). New islands of proliferating chondrocytes and a shortened distance between opposing cartilage end plates indicated cartilage regeneration. To assess whether or not this phenotype was limited to the treatment site, we topically treated one ear with imiquimod or control cream and injured the contralateral ear in WT mice. Compared with control-treated mice, imiquimod-treated mice healed their contralateral ear holes to a significantly smaller size, often achieving full ear hole closure (Fig. 1E). Next, to determine the optimal timing of treatment, we initiated topical imiquimod 5 days prior to and immediately after skin injury

and observed improved ear hole closure when treatment was initiated 5 days prior to skin injury (Fig. 1F). Taken together, these findings suggest that topical imiquimod treatment, initiated 5 days prior to injury, induces a circulating factor that promotes full-thickness tissue regeneration.

To determine if our observation is generalizable to other modes of injury, we studied a second model of mammalian tissue regeneration in which we treated the uninjured ears of WT mice with topical 5% imiquimod or control cream and performed the WIHN assay on the dorsal back skin (Fig. 1G) (8). Compared with control-treated mice, imiquimod-treated mice exhibited a 15-fold increase in the number of regenerated hair follicles. Thus, topical imiquimod treatment of adult mouse ear skin promoted tissue regeneration and organogenesis on injured back skin. Whereas large skin excisions stimulate wound-induced hair follicle neogenesis, smaller skin excisions typically heal with a scar. To test whether imiquimod would reduce scar formation, we created small skin wounds on dorsal back skin of WT mice and treated the skin surrounding the wound with 5% imiquimod or control cream (15). Compared with control-treated mice, imiquimod-treated mice achieved complete wound closure at a slower speed but healed with 6-fold smaller scars (Fig. S2). The use of these three mammalian wound-healing models demonstrate that topical imiquimod-treatment promotes systemic full-thickness tissue regeneration and/or reduces scar formation.

Imiquimod activates TRPA1 nociceptor to promote tissue regeneration

Imiquimod activates several other receptors in addition to TLR7 (Fig. 2A) (16–20). To identify which receptor may be responsible for promoting tissue regeneration, we treated mice genetically deficient in TLR7, MYD88, NLRP3, TRPV1, or TRPA1 with topical imiquimod or a control treatment. Relative to the control, topical imiquimod treatment continued to improve ear hole closure in strains deficient in TLR7, MYD88, NLRP3, and TRPV1 (Fig. 2B, 2C, S3A, S3B). Additionally, we treated WT mice with topical resiquimod, a more potent TLR7 specific agonist, at the site of injury, and did not observe improved ear hole closure compared with control (Fig. S3C) (17, 21). Thus, imiquimod-mediated tissue regeneration does not require TLR7, MYD88, NLRP3, or TRPV1.

The TRPA1 receptor appeared to mediate the regenerative effects of imiquimod, because TRPA1-deficient mice did not demonstrate improved ear hole closure after imiquimod treatment (Fig. 2D, 2E, S3D). Ear wounds in TRPA1-deficient mice treated with imiquimod healed with scars and without cartilage regeneration, compared with heterozygous littermate controls that regenerated their wounds after imiquimod treatment (Fig. 2F). We further verified the effect of TRPA1 activation by using allyl isothiocyanate (AITC), a well-characterized specific pharmacologic agonist of TRPA1 (22). Similar to imiquimod treatment, topical AITC treatment improved ear hole closure in WT mice, in some cases leading to complete ear hole closure (Fig. 2G), and this benefit was lost in TRPA1-deficient mice (Fig. 2G).

TRPA1 is a member of the transient receptor potential (TRP) superfamily of cation channels and is expressed in peripheral skin afferent neurons, which have cell bodies in the dorsal root ganglion and extend dendrites to innervate the skin (23). Previous studies have demonstrated

that imiquimod directly induces calcium influx in TRPA1-expressing cells and neurons (19, 24). Controversy exists around whether TRPA1 is also expressed in keratinocytes and/or immune cells, with these results mostly based on protein staining with antibodies (25–27). At the gene expression level, we were unable to detect TRPA1 mRNA by quantitative PCR in mouse skin or immune cells (Fig. 2H). Overall, these findings are consistent with the notion that topical imiquimod activates TRPA1 expressed on cutaneous peripheral sensory neurons to promote full-thickness tissue regeneration.

Activated TRPA1 induces the type 17 innate immune axis to promote tissue regeneration

TRP family receptor activation leads to inflammation in the skin by stimulating dermal dendritic cells (DDC) to produce IL-23, which in turn activates type 17 innate immune cells to produce IL-17A and IL-22 (16, 28, 29). We assessed whether TRPA1-mediated tissue regeneration may utilize this pathway. Injured WT mice exhibited elevated protein levels of IL-17A, IL-22, and IL-23 in wound edge tissue from imiquimod-treated mice compared with controls, and this protein induction was not seen in imiquimod-treated TRPA1-deficient mice (Fig. 3A). Similarly, in the serum, protein levels of IL-17A were elevated after injury in WT mice treated with imiquimod but not in TRPA1-deficient mice treated with imiquimod (Fig. 3B). To test whether DDCs were necessary for TRPA1-mediated tissue regeneration, we injected diphtheria toxin into CD11c-diphtheria toxin receptor (DTR) mice and confirmed *in vivo* depletion of DDCs by flow cytometry (Fig. S4A) (30). Compared with control, imiquimod treatment did not improve ear hole closure in DDC-depleted mice (Fig. 3C). We also assessed whether IL-23 was essential for TRPA1-mediated tissue regeneration, and imiquimod treatment did not enhance ear hole closure in IL-12p40-deficient mice (functionally IL-23 deficient) compared with control (Fig. 3D). These results reveal that TRPA1-mediated tissue regeneration requires systemic activation of type 17 innate immunity.

To test whether exogenous IL-23 could rescue tissue regeneration in TRPA1-deficient animals, we injected recombinant IL-23 protein subcutaneously near the wounded ears of TRPA1-deficient mice on a daily basis. These mice regained their ability to close imiquimod-treated injured ear holes (Fig. 3E). This finding supports a model in which TRPA1 activation promotes tissue regeneration through DDC-secreted IL-23, which in turn activates IL-17-producing cells.

Immunodeficient *Scid* (B- and T cell deficient) and *Foxn1*$^{-/-}$ (T cell deficient) mice were treated with topical imiquimod in the ear hole injury model in order to identify the downstream IL-17-producing immune cells. Compared with control WT mice, imiquimod treatment did not improve ear hole closure in either mouse strain (Fig. 3F, 3G), indicating that TRPA1-mediated tissue regeneration requires T cells.

TRPA1-mediated tissue regeneration requires γδ T cells

Immunohistochemistry and flow cytometry of wound-edge tissue revealed that imiquimod-treatment induced more recruitment of dermal CD3+ T cells to the injured area compared with control (Fig. 4A–C, S5A). We further defined the T cell subtype. We did not detect significant recruitment of αβ T cells, including Th17 cells, and noted that the majority of

recruited cells were dermal γδ T cells (Fig. 4C). Multiple groups have demonstrated that dermal γδ T cells are the primary producers of IL-17 in the skin (16, 31). Compared with control treatment, imiquimod treatment induced an approximately 3-fold increase of γδ T cells in wound-edge tissue of WT mice (Fig. 4D, S5B), and this recruitment was reduced and not statistically significant in TRPA1-deficient mice (Fig. 4D, S5A). Next, we investigated whether γδ T cells are required for TRPA1-mediated ear hole closure. In γδ T cell- (*Tcrd*$^{-/-}$) deficient mice, imiquimod treatment did not promote ear hole closure (Fig. 4E). This result is consistent with our prior studies indicating that dermal γδ T cells are required for WIHN (32). We also confirmed that dermal γδ T cells express the IL-23 receptor (Fig. S5C) (31). Taken together, TRPA1-mediated tissue regeneration requires dermal γδ T cells.

Interestingly, we examined gene expression data of ear hole wound-edge tissue from *Acomys*, a rodent-like species with enhanced skin regeneration properties (6, 33), and identified higher levels of γδ T cell receptor transcripts compared with controls (Fig. 4F). This suggests that other mammalian models of tissue regeneration may also utilize the γδ T cell mechanism.

Discussion

Our results reveal that TRPA1 activation in mammalian skin promotes local and distant tissue regeneration and reduces scar formation (Fig. 4G). Skin injury alone does not activate TRPA1 or type 17 innate immunity, which may help to explain why humans invariably heal skin wounds with scar formation. Prior studies suggested that nonspecific inflammation induced by numerous different stimuli, including imiquimod, modulates future epithelial skin stem cell behavior (34); however, treatment with other inflammatory stimuli did not promote tissue regeneration in our model (Fig. S1).

γδ T cells are a subtype of T cells and consist of two subpopulations: epidermal γδ T cells (also known as Dendritic Epidermal T cell, DETC) and dermal γδ T cells (35, 36). DETCs take up residence in the skin during embryogenesis and remain sessile in adult life, whereas dermal γδ T cells exhibit migratory behaviors and may circulate through lymph nodes and blood to inflamed tissues (37, 38). Our data supports the conclusion that TRPA1 is required for the imiquimod-stimulated recruitment of IL-17 producing dermal γδ T cells. We propose that local activation of TRPA1 primes dermal γδ T cells to respond to local and distant sites of skin injury. γδ T cells are known to promote tissue regeneration through secretion of Fgf9 (32), which may mediate the downstream γδ T cell-driven effects.

TRPA1-expressing sensory neurons are thought to be a subset of TRPV1-expressing sensory neurons (23). An unexpected finding in our study is the specificity of TRPA1, and not TRPV1, to promote tissue regeneration. However, we see functional, temporal, and spatial differences between imiquimod-induced TRPA1 and TRPV1 activation. In TRPV1-deficient mice, imiquimod induced skin inflammation is reduced, but these mice still completely heal their injured ear holes. TRPA1-deficient mice display the opposite behavior; imiquimod induced skin inflammation still occurs, but injured ear holes heal with a scar and stay open. Temporally, TRPV1-mediated skin inflammation occurs within 3–5 days, and TRPA1-

mediated tissue regeneration occurs over one month. Finally, in contrast to TRPA1, activated TRPV1+ cutaneous neurons mediate local activation of dermal γδ T cells but not in distant locations (23, 28). Whereas both TRPA1-mediated and TRPV1-mediated pathways ultimately activate dermal γδ T cells via IL-23, these differences suggest that additional downstream specificity must be encoded by these receptors. One possibility is that TRPA1 activation may stimulate a second signaling pathway specific to TRPA1. Alternatively, cell type specificity may also account for these differences, as TRPA1 is expressed only on sensory neurons, and TRPV1 is widely expressed on multiple cell types. Future experiments are needed to understand TRP receptor mediated specificity.

Scar formation and tissue regeneration are not mutually exclusive programs, and wounds may heal with a combination of both processes. TRPA1-activation promoted tissue regeneration and reduced scar formation in the ear hole and WIHN models and reduced scar formation in the smaller skin wound model. We speculate that the absence of tissue regeneration in the smaller skin wound model may be attributed to the speed of wound closure. Tissue regeneration in the ear hole and WIHN models is slow and occurs over one month, whereas smaller skin excisions heal within 8–10 days primarily through wound contraction. Thus, the window for TRPA1-activation to promote regeneration of original skin appendages may be too short. Future studies will assess the relationship between the speed of wound healing, tissue regeneration, and scar formation.

Some limitations of our study include whether this TRPA1-mediated pathway may reduce fibrosis in epithelial tissues other than skin, and whether this pathway performs similar functions in the skin of other species. Human skin contains fewer γδ T cells during homeostasis compared to mouse skin, but humans do carry an equivalent dermal γδ T cell population that is biased to secrete IL-17 and has been implicated to play a role in disease pathophysiology (39). Our results suggest that randomized clinical trials testing topical 5% imiquimod cream and other TRPA1 agonists and activators of the type 17 innate immune pathway to promote tissue regeneration and prevent scar formation in humans may be warranted.

Study Design

We predefined study components including rules for stopping data collection, data inclusion/exclusion criteria, and endpoint selection methods. Specific information is described in their relevant section. The overall objective of our study was to identify methods to reduce scar formation and to promote tissue regeneration in mammals. We used *in vivo* mouse models, mouse genetics, and molecular biology to study this question. Presented data combines all experiments, and unless noted, all experiments were repeated at least two times independently. Animals used in this study were randomly assigned to experimental groups, and investigators were not blinded to allocation during experiments and outcome assessment, unless noted in the text.

Methods and Materials

Animals

C57BL/6 mice (strain #664), B6129PF2/J (strain #100903), *Trpa1*$^{-/-}$ (strain #6401), *Tlr7*$^{-/-}$ (strain #8380), *Trpv1*$^{-/-}$ (strain #3770), *Il-12p40*$^{-/-}$ (strain #2693), *Tcrd*$^{-/-}$ (strain #2120), *Myd88*$^{-/-}$ (strain #9088), *Nlrp3*$^{-/-}$ (strain # 21302), *CD11c-DTR/GFP* (strain #4509), *Scid* (strain #1913), and *Foxn1*$^{-/-}$ *J:NU* (strain #7850) were purchased from The Jackson Laboratory. All mice were group housed in the animal facility of University of Pennsylvania on a 12-hour light/12-hour dark cycle with ad libitum access to water and normal chow. Mice were verified by genotyping. The CD11c-DTR/GFP transgenic line has the CD11c promoter directing expression of a diphtheria toxin receptor - enhanced green fluorescent protein (DTR/EGFP) fusion protein to dendritic cell populations. To deplete dendritic cell populations, we administered diphtheria toxin intraperitoneal (100ng per mouse) 3 times per week. Mice used in this study were male and female age-matched and background-matched littermates that were randomly assigned to experimental groups. No sex-dependent differences were observed.

Study approval

Experiments involving mice were reviewed and approved by the Institutional Animal Care and Use Committee of University of Pennsylvania. Mice were treated in accordance with the NIH guidelines for the humane care of animals.

Injury Models

We applied ~50mg of imiquimod 5% cream (Perrigo), Calcipotriene cream 0.005% (Prasco), or 100% acetone (Sigma) to one or both ears of a mouse 5 times per week. Control was bland cream (Cetaphil ® Moisturizing Cream). For compounded IMQ experiments, we purchased imiquimod powder (Sigma) and spatulated the powder into Cetaphil cream. For AITC experiments, we used 5% AITC diluted in mineral oil and applied 1–2 drops per ear 3 days a week. Control was mineral oil. For the recombinant IL-23 experiment, 500ng of IL-23 (Sigma), diluted in PBS, was injected subcutaneously at the base of each ear daily for the entire duration of the experiment. Vehicle control was PBS. For ear wounding, we used a standard 2mm mechanical punch (Roboz, Gaithersburg, MD) to create a hole in the center of each outer ear (pinna). Ear hole diameter was measured using a dissection microscope (Nikon) in the horizontal and vertical directions on a weekly basis. Ears were excluded if there were signs of wound infection, tearing of the ear, or abnormal geometric shape. Hole size for the right ear are reported. For the smaller skin excision model, we used a standard 6mm mechanical punch (Acuderm) to create a full-thickness hole in the dorsal back skin. We confirmed the presence of scar by the flattening of rete ridges, horizontal oriented collagen bundles, and absence of skin appendages. To calculate scar area, we sectioned through the entire tissue block to identify the section containing the longest scar diameter as measured as the distance between intact hair follicles. We measured dermal thickness from the base of the epidermis to the subcutaneous fat. These criteria were pre-established.

Histology and Immunohistochemistry

Standard histology and immunostaining protocols were performed, and investigators were blinded during histologic staining. 4% paraformaldehyde was used as the fixative. Briefly, immunohistochemical analysis was performed on 5–10 μm-thick sections of mouse skin. The following primary antibodies were used: rabbit polyclonal anti–keratin 14 (1:100; BioLegend), rabbit polyclonal anti–CD3 (1:100; BioLegend or Abcam #5690), and hamster monoclonal anti-TCRD (1:500; BioLegend). Immune complexes were detected with secondary antibodies conjugated with either GFP (Abcam). After staining, images were directly analyzed using a Leica Microsystems DM6 B microscope equipped with a DFC9000 Camera or Keyence imaging system. A minimum of 4–6 sections was stained per sample. Secondary only control was included for every experiment. Unwounded skin was included as a control for each antibody. Representative images selected for figure panels.

RNAscope (ACD Bio) was performed on fresh frozen control ears and brain tissue as per manufacturer's protocols. Cy3-TSA fluorophore (Perkin Elmer) was used to visualize the following probes: DapB of Bacillus subtilis strain (negative control), POLR2A (positive control), and Trpa1–01. Images were acquired using a Leica microscope.

Flow Cytometry

For immune cell recruitment experiments, freshly dissected tissue from the rim of healing wounds were manually dissociated with scissors and then incubated with Liberase TL (Roche) for 90 min at 37°C. After dissociation, cells were washed in PBS and resuspended in FACS buffer (PBS + 0.05% NaN3 + 2% FBS). The following primary antibodies were used: anti-mouse CD3-FITC antibody (BioLegend), anti-mouse CD45-Pacific Blue antibody (BioLegend), anti-mouse $\gamma\delta$ TCR-APC (Biolegend), anti-mouse CD4-APC, anti-mouse CD8-BV650 (BioLegend), and TCR Vγ3-PE (BioLegend). 7-AAD (BioLegend) was added to exclude dead cells. The CD11c-DTR/GFP transgenic line (#4509) introduces endogenous GFP expression in dendritic cell populations, and we used this GFP marker to monitor dendritic cell depletion.

Cell sorting was performed at the Flow Cytometry and Cell Sorting Facility (University of Pennsylvania). Standard FACS procedures were performed. The BD™ CompBeads Set Anti-Mouse Ig, κ or isolated mouse spleen cells were used to compensate and determine gating strategies. Fluorescence expression was quantified with FlowJo software (Treestar).

ELISA

Blood was obtained from the retro-orbital sinus, and serum was collected after blood coagulation. Wound edge tissue was collected in RIPA buffer and homogenized in the FastPrep instrument (Fastprep 24, Lysing Matrix D, MP Bio) per manufacturer's protocol. The Bradford assay was performed to measure protein concentration of each sample. Serum and tissue IL-17A, IL-22, and IL-23 ELISAs were performed per the manufacturer's instructions (Biolegend). Recombinant IL-17A, IL-22, or IL-23 was used as a positive control (Biolegend).

Real-time RT–PCR

Freshly dissected tissue from the rim of healing appendages were manually dissociated with scissors, collected in TRI Regeant (Zymo) and then mechanically disrupted (Fastprep 24, Lysing Matrix D, MP Bio). Total RNA was isolated by Direct-Zol RNA MicroPrep (Zymo). RNA concentration was measured by Nanodrop 1000 (Thermo Scientific). cDNA synthesis was performed with Maxima Reverse Transcriptase (Thermo Scientific) or Superscript IV VILO (Thermo Scientific) per manufacturer's instructions. One-step quantitative RT–PCR was performed and analyzed using an ABI ViiA7 Real-Time PCR detection system (Applied Biosystems) with TaqMan one-step RT–PCR Master Mix Reagents. Taqman probes were purchased for mouse *Il-23r, beta-actin, and Trpa1* (Applied Biosystems).

Wound Induced Hair Neogenesis

1-cm2 full-thickness skin wounds were made as previously described (Ito *et al.*, 2007). 5-weeks later, de novo hair follicles were identified by whole-mount alkaline phosphatase staining of dermis preparations as previously described (Ito *et al.*, 2007).

Statistical Analysis

For *in vivo* time courses comparing hole size (Fig. 1B, 1E, 1F, 1G, 1H, 2A, 1C, 2D, 2E, 3C, 3D, 3E, 3F, 3G, 3H, 4E, S1A, S2B, S2C, S2D), data were each analyzed using a parametric and a non-parametric method. The choice of the parametric method is a 2-way analysis of variance (ANOVA) using a temporal main effect, a main effect comparing treatment, and an interaction of the two main effects. The non-parametric method is a Friedman rank sum test with replicated blocks. In the Friedman test, groups are defined by treatments and blocks are times. No interaction is allowed in the Friedman test. For tests such that the two-way ANOVA indicates significant time-treatment interactions, additionally 2-tailed Student's *t* test was used, with *P* values of less than 0.05 considered significant. The conclusions for the test between treatments using the two methods are identical, except for in Fig. 3C, where the non-parametric test is significant (p=0.03) while the parametric test is not (p=0.16). The difference can be attributed to the fact that the 2-way ANOVA has less power due to its inclusion of an interaction term between treatment and time. Otherwise, 2-tailed Student's t test was used to determine significance, with *P value*s of less than 0.05 considered significant. Higher levels of significance are indicated by the following: ** $P < 0.01$, *** $P<0.001$ in the text.

Supplementary Material

Refer to Web version on PubMed Central for supplementary material.

Acknowledgments:

We thank M. Lazar, W. Luo, E. Morrisey, T. Ridky, K. Zaret, and members of the Leung Lab for careful reading of the manuscript. S. Prouty, J. Seykora, and the Skin Biology Disease Resource Center for technical support.

Funding: T.H.L. receives support from NIH (K08-AR066661, P30-AR069589), VA (I01RX002701), Moseley Foundation, Edwin and Fanny Gray Hall Center for Human Appearance, and H.T. Leung Foundation.

References and Notes:

1. Sun BK, Siprashvili Z, Khavari PA, Advances in skin grafting and treatment of cutaneous wounds, Science 346, 941–945 (2014). [PubMed: 25414301]
2. Marshall CD, Hu MS, Leavitt T, Barnes LA, Lorenz HP, Longaker MT, Cutaneous Scarring: Basic Science, Current Treatments, and Future Directions, Advances in Wound Care 7, 29–45 (2018). [PubMed: 29392092]
3. Bedelbaeva K, Snyder A, Gourevitch D, Clark L, Zhang XM, Leferovich J, Cheverud JM, Lieberman P, Heber-Katz E, Lack of p21 expression links cell cycle control and appendage regeneration in mice, Proc Natl Acad Sci USA 107, 5845–5850 (2010). [PubMed: 20231440]
4. Leung TH, Snyder ER, Liu Y, Wang J, Kim SK, A cellular, molecular, and pharmacological basis for appendage regeneration in mice, Genes Dev 29, 2097–2107 (2015). [PubMed: 26494786]
5. Zhang G, Li J, Purkayastha S, Tang Y, Zhang H, Yin Y, Li B, Liu G, Cai D, Hypothalamic programming of systemic ageing involving IKK-β, NF-κB and GnRH, Nature 497, 211–216 (2013). [PubMed: 23636330]
6. Seifert AW, Kiama SG, Seifert MG, Goheen JR, Palmer TM, Maden M, Skin shedding and tissue regeneration in African spiny mice (Acomys), Nature 489, 561–565 (2012). [PubMed: 23018966]
7. Ito M, Yang Z, Andl T, Cui C, Kim N, Millar SE, Cotsarelis G, Wnt-dependent de novo hair follicle regeneration in adult mouse skin after wounding, Nature 447, 316–320 (2007). [PubMed: 17507982]
8. Clark LD, Clark RK, Heber-Katz E, A new murine model for mammalian wound repair and regeneration, Clin. Immunol. Immunopathol 88, 35–45 (1998). [PubMed: 9683548]
9. Gourevitch DL, Clark L, Bedelbaeva K, Leferovich J, Heber-Katz E, Dynamic changes after murine digit amputation: the MRL mouse digit shows waves of tissue remodeling, growth, and apoptosis, Wound Repair Regen 17, 447–455 (2009). [PubMed: 19660054]
10. Gourevitch D, Clark L, Chen P, Seitz A, Samulewicz SJ, Heber-Katz E, Matrix metalloproteinase activity correlates with blastema formation in the regenerating MRL mouse ear hole model, Dev. Dyn 226, 377–387 (2003). [PubMed: 12557216]
11. Heber-Katz E, Zhang Y, Bedelbaeva K, Song F, Chen X, Stocum DL, Cell cycle regulation and regeneration, Curr. Top. Microbiol. Immunol 367, 253–276 (2013). [PubMed: 23263201]
12. Nishiguchi MA, Spencer CA, Leung DH, Leung TH, Aging Suppresses Skin-Derived Circulating SDF1 to Promote Full-Thickness Tissue Regeneration, CellReports 24, 3383–3392.e5 (2018).
13. Eming SA, Wynn TA, Martin P, Inflammation and metabolism in tissue repair and regeneration, Science 356, 1026–1030 (2017). [PubMed: 28596335]
14. Sidgwick GP, McGeorge D, Bayat A, A comprehensive evidence-based review on the role of topicals and dressings in the management of skin scarring, Archives of Dermatological Research 307, 461–477 (2015). [PubMed: 26044054]
15. Lim CH, Sun Q, Ratti K, Lee S-H, Zheng Y, Takeo M, Lee W, Rabbani P, Plikus MV, Cain JE, Wang DH, Watkins DN, Millar S, Taketo MM, Myung P, Cotsarelis G, Ito M, Hedgehog stimulates hair follicle neogenesis by creating inductive dermis during murine skin wound healing, Nature Communications 9, 1–13 (2018).
16. Riol-Blanco L, Ordovas-Montanes J, Perro M, Naval E, Thiriot A, Alvarez D, Paust S, Wood JN, von Andrian UH, Nociceptive sensory neurons drive interleukin-23- mediated psoriasiform skin inflammation, Nature 510, 157–161 (2014). [PubMed: 24759321]
17. Hemmi H, Kaisho T, Takeuchi O, Sato S, Sanjo H, Hoshino K, Horiuchi T, Tomizawa H, Takeda K, Akira S, Small anti-viral compounds activate immune cells via the TLR7 MyD88-dependent signaling pathway, 3, 196–200 (2002).
18. Kanneganti T-D, Ozören N, Body-Malapel M, Amer A, Park J-H, Franchi L, Whitfield J, Barchet W, Colonna M, Vandenabeele P, Bertin J, Coyle A, Grant EP, Akira S, Núñez G, Bacterial RNA and small antiviral compounds activate caspase-1 through cryopyrin/Nalp3, Nature 440, 233–236 (2006). [PubMed: 16407888]
19. Kemény Á, Kodji X, Horváth S, Komlódi R, Szőke É, Sándor Z, Perkecz A, Gyömörei C, Sétáló G, Kelemen B, Bíró T, Tóth BI, Brain SD, Pintér E, Gyulai R, TRPA1 Acts in a Protective Manner

in Imiquimod-Induced Psoriasiform Dermatitis in Mice, J Invest Dermatol 138, 1774–1784 (2018). [PubMed: 29550417]

20. Zhou Y, Han D, Follansbee T, Yu S, Wang B, Shi Z, Domocos DT, Carstens M, Carstens E, Hwang ST, Transient receptor potential ankyrin 1 (TRPA1) positively regulates imiquimod-induced, psoriasiform dermal inflammation in mice, J Cell Mol Med 31, 205–10 (2019).
21. Jurk M, Heil F, Vollmer J, Schetter C, Krieg AM, Wagner H, Lipford G, Bauer S, Human TLR7 or TLR8 independently confer responsiveness to the antiviral compound R-848, 3, 499–499 (2002). [PubMed: 12032557]
22. Jordt S-E, Bautista DM, Chuang H-H, McKemy DD, Zygmunt PM, Högestätt ED, Meng ID, Julius D, Mustard oils and cannabinoids excite sensory nerve fibres through the TRP channel ANKTM1, Nature 427, 260–265 (2004). [PubMed: 14712238]
23. Story GM, Peier AM, Reeve AJ, Eid SR, Mosbacher J, Hricik TR, Earley TJ, Hergarden AC, Andersson DA, Hwang SW, McIntyre P, Jegla T, Bevan S, Patapoutian A, ANKTM1, a TRP-like channel expressed in nociceptive neurons, is activated by cold temperatures, Cell 112, 819–829 (2003). [PubMed: 12654248]
24. Esancy K, Condon L, Feng J, Kimball C, Curtright A, Dhaka A, A zebrafish and mouse model for selective pruritus via direct activation of TRPA1, eLife 7, 13819 (2018).
25. Denda M, Tsutsumi M, Goto M, Ikeyama K, Denda S, Topical Application of TRPA1 Agonists and Brief Cold Exposure Accelerate Skin Permeability Barrier Recovery, J Invest Dermatol 130, 1942–1945 (2010). [PubMed: 20182443]
26. Zappia KJ, Garrison SR, Palygin O, Weyer AD, Barabas ME, Lawlor MW, Staruschenko A, Stucky CL, Beggs S, Ed. Mechanosensory and ATP Release Deficits following Keratin14-Cre-Mediated TRPA1 Deletion Despite Absence of TRPA1 in Murine Keratinocytes, PLoS ONE 11, e0151602–30 (2016). [PubMed: 26978657]
27. Atoyan R, Shander D, Botchkareva NV, Non-neuronal expression of transient receptor potential type A1 (TRPA1) in human skin, J Invest Dermatol 129, 2312–2315 (2009). [PubMed: 19282836]
28. Cohen JA, Edwards TN, Liu AW, Hirai T, Jones MR, Wu J, Li Y, Zhang S, Ho J, Davis BM, Albers KM, Kaplan DH, Cutaneous TRPV1+ Neurons Trigger Protective Innate Type 17 Anticipatory Immunity, Cell 178, 919–932.e14 (2019). [PubMed: 31353219]
29. Kashem SW, Riedl MS, Yao C, Honda CN, Vulchanova L, Kaplan DH, Nociceptive Sensory Fibers Drive Interleukin-23 Production from CD301b+ Dermal Dendritic Cells and Drive Protective Cutaneous Immunity, Immunity 43, 515–526 (2015). [PubMed: 26377898]
30. Jung S, Unutmaz D, Wong P, Sano G-I, De los Santos K, Sparwasser T, Wu S, Vuthoori S, Ko K, Zavala F, Pamer EG, Littman DR, Lang RA, In vivo depletion of CD11c+ dendritic cells abrogates priming of CD8+ T cells by exogenous cell-associated antigens, Immunity 17, 211–220 (2002). [PubMed: 12196292]
31. Cai Y, Shen X, Ding C, Qi C, Li K, Li X, Jala VR, Zhang H-G, Wang T, Zheng J, Yan J, Pivotal Role of Dermal IL-17-Producing γδ T Cells in Skin Inflammation, Immunity 35, 596–610 (2011). [PubMed: 21982596]
32. Gay D, Kwon O, Zhang Z, Spata M, Plikus MV, Holler PD, Ito M, Yang Z, Treffeisen E, Kim CD, Nace A, Zhang X, Baratono S, Wang F, Ornitz DM, Millar SE, Cotsarelis G, Fgf9 from dermal γδ T cells induces hair follicle neogenesis after wounding, Nat Med 19, 916–923 (2013). [PubMed: 23727932]
33. Gawriluk TR, Simkin J, Thompson KL, Biswas SK, Clare-Salzler Z, Kimani JM, Kiama SG, Smith JJ, Ezenwa VO, Seifert AW, Comparative analysis of ear-hole closure identifies epimorphic regeneration as a discrete trait in mammals, Nature Communications 7, 1–16 (2016).
34. Naik S, Larsen SB, Gomez NC, Alaverdyan K, Sendoel A, Yuan S, Polak L, Kulukian A, Chai S, Fuchs E, Inflammatory memory sensitizes skin epithelial stem cells to tissue damage, Nature 550, 1–20 (2017).
35. Havran WL, Grell S, Duwe G, Kimura J, Wilson A, Kruisbeek AM, O'Brien RL, Born W, Tigelaar RE, Allison JP, Limited diversity of T-cell receptor gamma-chain expression of murine Thy-1+ dendritic epidermal cells revealed by V gamma 3-specific monoclonal antibody, Proceedings of the National Academy of Sciences 86, 4185–4189 (1989).

36. Suwanpradid J, Holcomb ZE, MacLeod AS, Emerging Skin T-Cell Functions in Response to Environmental Insults, J Invest Dermatol 137, 288–294 (2017). [PubMed: 27784595]

37. Sumaria N, Roediger B, Ng LG, Qin J, Pinto R, Cavanagh LL, Shklovskaya E, Fazekas B de St Groth, J. A. Triccas, W. Weninger, Cutaneous immunosurveillance by self-renewing dermal γδ T cells, Journal of Experimental Medicine 208, 505–518 (2011). [PubMed: 21339323]

38. Ramírez-Valle F, Gray EE, Cyster JG, Inflammation induces dermal Vγ4+ γδT17 memory-like cells that travel to distant skin and accelerate secondary IL-17-driven responses, Proc Natl Acad Sci USA 112, 8046–8051 (2015). [PubMed: 26080440]

39. O'Brien RL, Born WK, Dermal γδ T cells--What have we learned? Cell. Immunol 296, 62–69 (2015). [PubMed: 25649119]

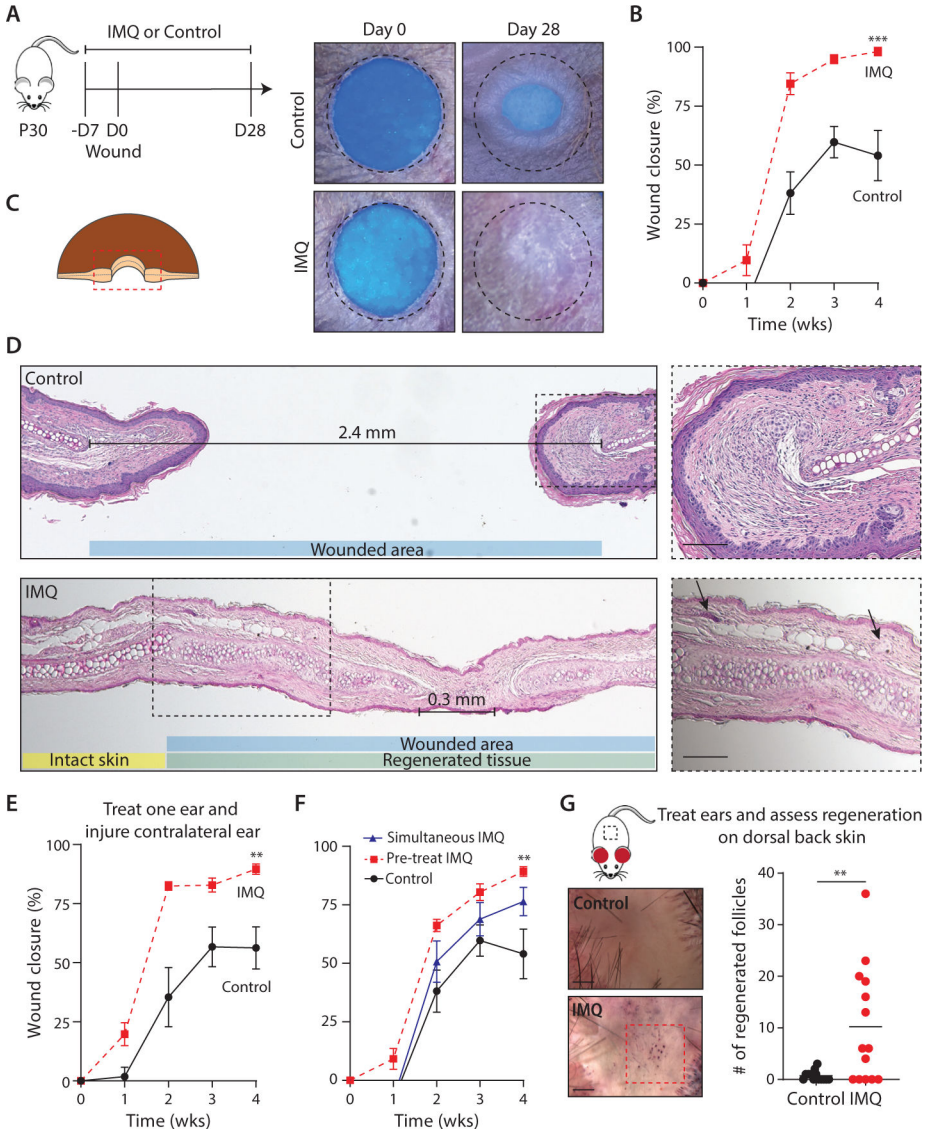

Figure 1: Imiquimod induces a circulating factor that promotes mammalian tissue regeneration.

(A) Representative photographs of control and imiquimod (IMQ)-treated WT ears. Dotted circle represents original 2mm hole-punch size.

(B) Percentage of wound closure in Cetaphil control- (solid black line) and IMQ-treated (dashed red line) WT mouse ears. *N=10*.

(C) Schematic of histology orientation.

(D) Representative Hematoxylin & Eosin stained tissue sections from control- and IMQ-treated WT mouse ears. Distance between opposing cartilage endplates are marked. Original wound size represented by blue box; Regenerated tissue represented by green box; Uninjured skin represented by yellow box. Higher magnification images from boxed areas. Arrows denote new hair follicles and sebaceous glands, which are further highlighted in inset images. *N=10*. Scale bars, 100μM.

(E) Percentage of wound closure in control- (solid black line) and IMQ- treated (dashed red line) WT mice, where one ear was treated and the contralateral ear was injured. *N=7* (control); N=*9* (IMQ).
(F) Percentage of wound closure in WT mice, where time of IMQ treatment initiation was varied. *N=7* (control); *N=8* (IMQ).
(G) Wound induced hair neogenesis (WIHN): representative images from control- and IMQ-treated dorsal back skin. Area of WIHN shown in red box. Quantification of regenerated follicle numbers. *N=14*. Scale bars, 1mm.
N=biological replicates per group. Data are pooled from at least two independent experiments. (B, E, and F) Two-way analysis of variance (ANOVA) and Friedman rank sum test with replicated blocks. (G) 2-tailed unpaired *t* test. Data presented are means ± SEM. ** P<0.01 and *** P<0.001.

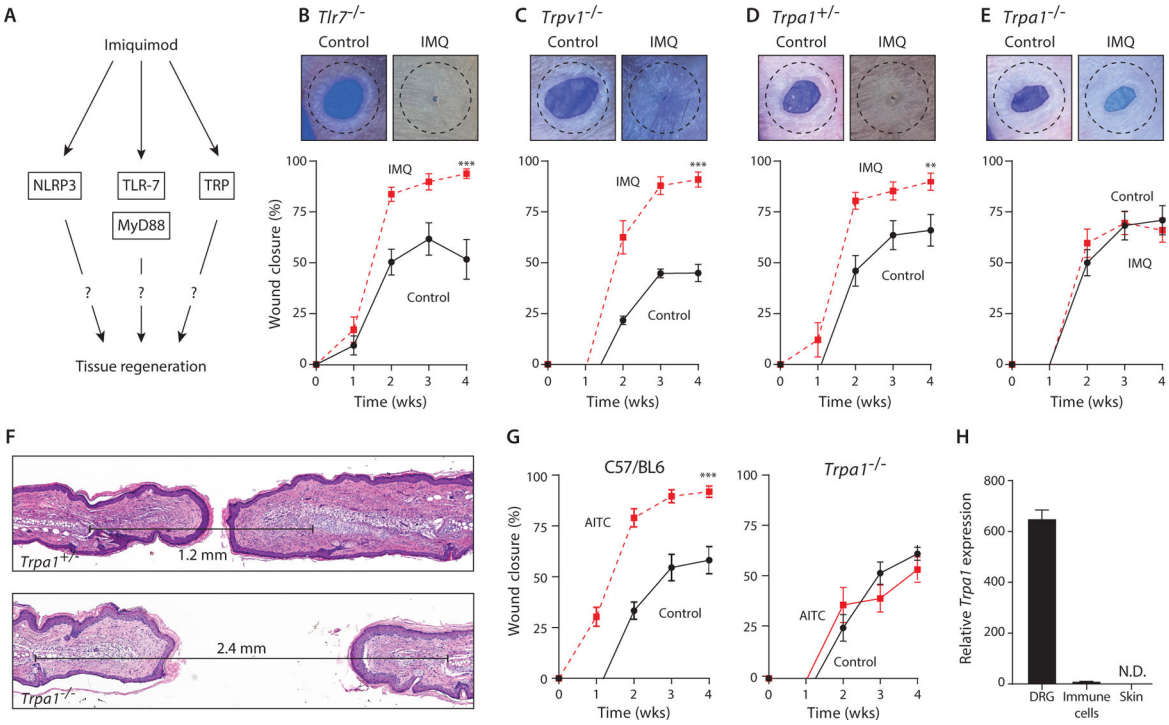

Figure 2: Activated TRPA1 nociceptor promotes tissue regeneration.

(A) Schematic of imiquimod (IMQ) signaling pathway.

(B-E) Representative photographs of ear holes 4 weeks after injury and percentage of wound closure in control- (solid black line) and IMQ-treated (dashed red line) mice. (b) *Tlr7*$^{-/-}$ mice. *N=4* (control); *N=9* (IMQ). (c) *Trpv1*$^{-/-}$ mice. *N=7*. (d) *Trpa1*$^{+/-}$ mice. *N=3* (control); *N=6* (IMQ). (e) *Trpa1*$^{-/-}$ mice. *N=9* (control); *N=15* (IMQ).

(F) Representative H&E stained sections from IMQ-treated *Trpa1*$^{-/-}$ and *Trpa1*$^{+/-}$ mice. Distance between cartilage endplates are marked.

(G) Percentage of wound closure in mineral oil control- (solid black line) and allyl isothiocyanate (AITC)-treated (dashed red line) WT (C57/BL6) and *Trpa1*$^{-/-}$ mice. C57/BL6 mice: *N=4. Trpa1*$^{-/-}$ mice: *N=7* (control); *N=6* (AITC).

(H) Relative value units of mouse TRPA1 transcript in different mouse tissues by qPCR. Dorsal root ganglion (DRG). *N=3* (DRG)*; N=5* (Immune cells and skin).

Dotted circle represents original 2mm-diameter hole size. *N*=biological replicates per group. Data are pooled from at least two independent experiments. (B, C, D, E, and G) Two-way analysis of variance (ANOVA) and Friedman rank sum test with replicated blocks. Data presented are means ± SEM. ** P<0.01 and *** P<0.001.

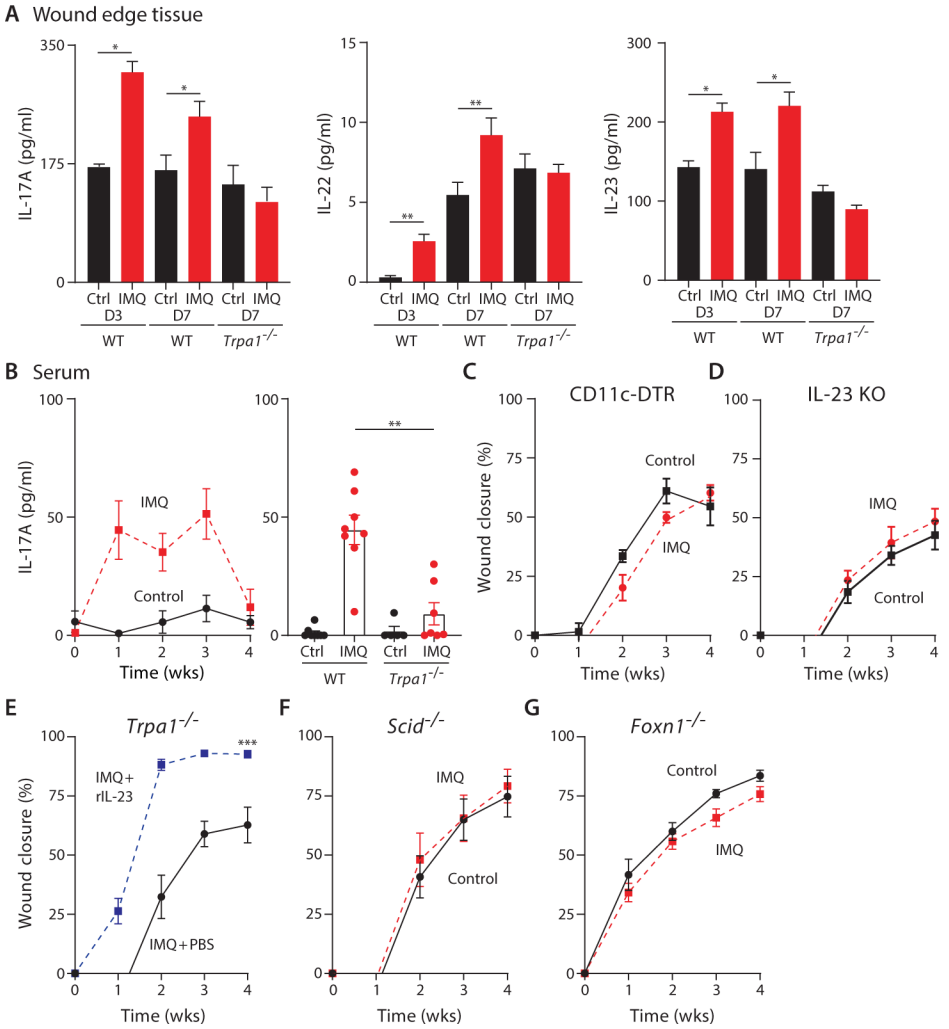

Figure 3: Activated TRPA1 induces the type 17 innate immune axis to promote tissue regeneration.

(A) IL-17, IL-22, and IL-23 protein levels in wound edge tissue isolated from control- (black bars) and imiquimod (IMQ)-treated (red bars) WT and *Trpa1*$^{-/-}$ mice. IL-17: *N=3* (WT D3); *N=8* (WT D7)*; N=4* (*Trpa1*$^{-/-}$ D7). IL-22: *N=3* (WT D3); *N=9* (WT D7)*; N=7* (*Trpa1*$^{-/-}$ D7). IL-23: *N=3* (WT D3); *N=4* (WT D7)*; N=6* (*Trpa1*$^{-/-}$ D7). (*) P<0.05; (**) P<0.01.

(B) Serum IL-17 protein levels from control- (solid black line) and IMQ-treated (dashed red line) WT and *Trpa1*$^{-/-}$ mice. Left panel, *N=5* (WT), *N=4* (*Trpa1*$^{-/-}$); Right panel, *N=8* (WT), *N=7* (*Trpa1*$^{-/-}$). (**) P<0.01.

(C) *CD11c-DTR* mice were treated with diphtheria toxin to deplete dendritic cells. Percentage of wound closure in control- (solid black line) and IMQ-treated mice (dashed red line). *N=6* (control)*; N=4* (IMQ).

(D) Percentage of wound closure in control- (solid black line) and IMQ-treated (dashed red line) *Il-12p40*$^{-/-}$ (functionally IL-23 deficient) mice. *N=7* (control)*; N=10* (IMQ).

(E) *Trpa1*$^{-/-}$ mice received daily subcutaneous injections of recombinant IL-23 (dashed blue line) or PBS (solid black line) near the ear. Percentage of wound closure in control- and IMQ-treated mice. *N=5* (PBS); *N=13* (recombinant IL-23).

(F) Percentage of wound closure in control- (solid black line) and IMQ-treated (dashed red line) *Scid*$^{-/-}$ mice. *N=5.*

(G) Percentage of wound closure in control- (solid black line) and IMQ-treated (dashed red line) *Foxn1*$^{-/-}$ mice. *N=5.*

N=biological replicates per group. Data are pooled from at least two independent experiments. (A and B) 2-tailed unpaired *t* test. (B-G) Two-way analysis of variance (ANOVA) and Friedman rank sum test with replicated blocks. Data presented are means ± SEM. * P<0.05, ** P<0.01, and *** P<0.001. For (C), p=.16 for ANOVA and p=0.03 for Friedman rank sum.

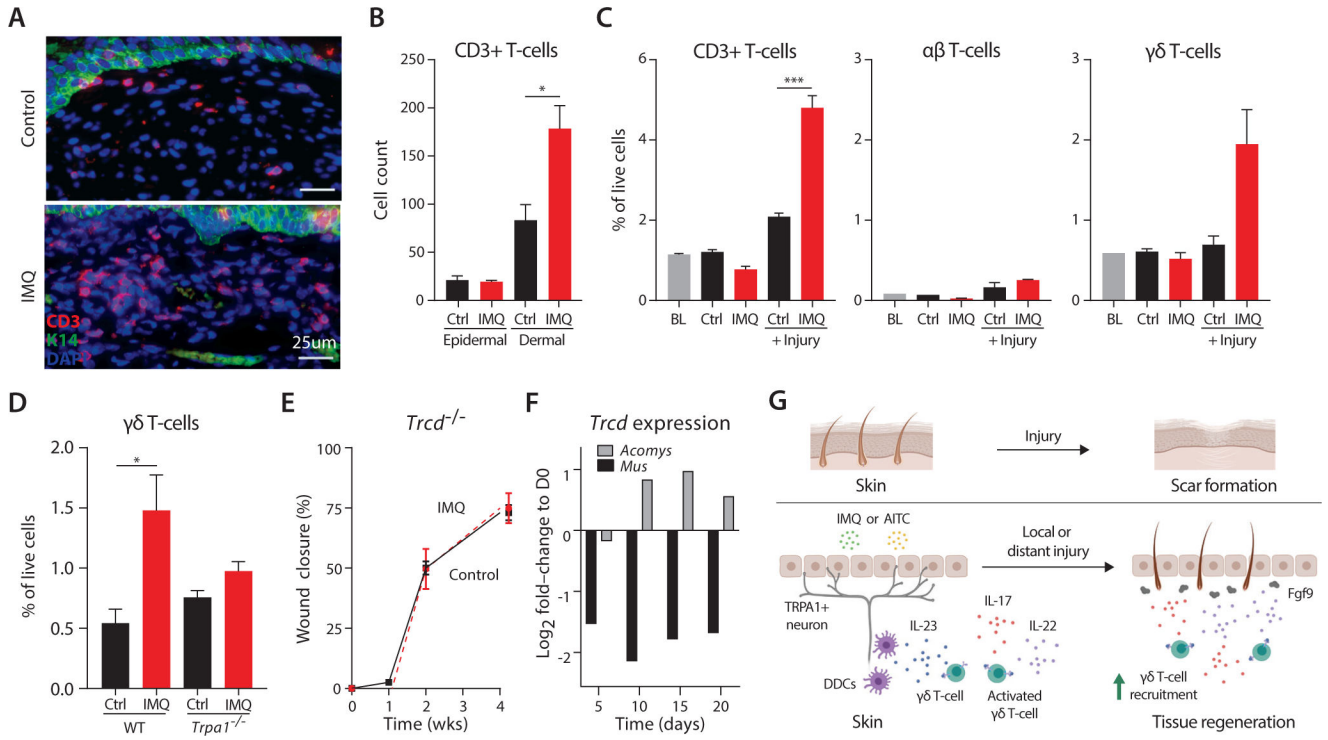

Figure 4: γδ T cells are required for TRPA1-mediated tissue regeneration.

(A) Representative immunofluorescence sections for CD3 (red), keratin-14 (green), and nuclei (blue) in control- and imiquimod (IMQ)-treated wound edge tissue from WT mice at day 7 after injury. Scale bars, 25μM.

(B) Quantification dermal and epidermal CD3 staining in control- and IMQ-treated ears. *N=3.*

(C) Percentage of CD3+ T cells, αβ T cells, and γδ T cells relative to total live cells in wound edge tissue from control- and IMQ-treated WT and *Trpa1*$^{-/-}$ mice. *N=5* (baseline); *N=6* (control and IMQ).

(D) Percentage of γδ T cells relative to total live cells in wound edge tissue taken at day 7 after injury from control- and IMQ-treated WT and *Trpa1*$^{-/-}$ mice. *N=5.*

(E) Percentage of wound closure in control- (solid black line) and IMQ-treated (dashed red line) *Tcrd*$^{-/-}$ mice. *N=6.*

(F) TCRD transcript assessed in injured wound edge tissue from non-regenerating *Mus musculus* mice and regenerating *Acomys* rodents. Data obtained from previously published analysis (33).

(G) Schematized model of neuroimmune-regeneration.

N=biological replicates per group. Data are pooled from at least two independent experiments. (B-D) 2-tailed unpaired *t* test. (E) Two-way analysis of variance (ANOVA) and Friedman rank sum test with replicated blocks. Data presented are means ± SEM. * P<0.05, ** P<0.01 and *** P<0.001.